

Studying protein–protein interaction through side-chain modeling method OPUS-Mut

Gang Xu , Yilin Wang, Qinghua Wang and Jianpeng Ma

Corresponding author: Jianpeng Ma, Multiscale Research Institute of Complex Systems, Fudan University, Shanghai, 200433, China. E-mail: jpma@fudan.edu.cn

Abstract

Protein side chains are vitally important to many biological processes such as protein–protein interaction. In this study, we evaluate the performance of our previous released side-chain modeling method OPUS-Mut, together with some other methods, on three oligomer datasets, CASP14 (11), CAMEO-Homo (65) and CAMEO-Hetero (21). The results show that OPUS-Mut outperforms other methods measured by all residues or by the interfacial residues. We also demonstrate our method on evaluating protein–protein docking pose on a dataset Oligomer-Dock (75) created using the top 10 predictions from ZDOCK 3.0.2. Our scoring function correctly identifies the native pose as the top-1 in 45 out of 75 targets. Different from traditional scoring functions, our method is based on the overall side-chain packing favorableness in accordance with the local packing environment. It emphasizes the significance of side chains and provides a new and effective scoring term for studying protein–protein interaction.

Keywords: protein side-chain modeling, protein–protein interaction, protein–protein docking, scoring protein–protein docking poses

Introduction

Protein–protein interaction is essential for many biological systems, and it is also important in designing peptidic drugs [1]. Many protein–protein interactions are mediated by amino-acid side chains, especially those of the interfacial residues [2]. Previous studies show that accurate modeling of side-chain conformations at the interface is necessary for high-resolution protein–protein docking [3] and protein–ligand docking [4]. Improving the side-chain modeling accuracy will generate more native-like distributions of intra-molecular and inter-molecular residue energies, which is beneficial to the protein docking task [3].

In recent years, many successful backbone-dependent side-chain modeling methods have been proposed [5–17]. The sampling-based methods select the rotamers from the rotamer library according to their search schemes and keep the best rotamer for each residue with the minimal score depending on their scoring functions. This kind of methods run fast, and they are suitable for the repeatedly applied side-chain modeling in the folding process, examples include SCWRL4 [14] and FASPR [16]. However, the performance is limited by the discrete rotamers in the rotamer library and the accuracy of the scoring function [6]. With the help of deep learning techniques, some new methods have been developed, which successfully capture the local environment of each residue using 3DCNN network and improve the accuracy of side-chain

modeling by a large degree. Examples include DLPacker [7] and OPUS-Mut [17].

Scoring protein–protein docking poses is another important task in studying protein–protein interaction. Various criteria [18] have been proposed, such as force-field-based criteria [19, 20], knowledge-based criteria [21, 22] and machine learning-based criteria [23–26]. For example, ZRANK utilizes a scoring function that includes van der Waals energies, electrostatics energies and desolvation energy [20]. GNN-DOVE is a recently developed graph neural network-based docking decoy evaluation score that can distinguish the near-native models from those incorrect decoys [25]. It is a binary classification model that is trained on the datasets that contains both near-native and incorrect decoys. Since the side chains of the residues, especially those located at the interface, are crucial for protein–protein interaction, a scoring term that is mainly based on side chains may be an effective term for better scoring the protein–protein docking poses.

In this paper, we use the structures of oligomers to study protein–protein interaction. We evaluate the side-chain modeling performance of our previous released method OPUS-Mut [17], along with some other methods, on three oligomer datasets collected in this study, CASP14 (11), CAMEO-Homo (65) and CAMEO-Hetero (21). The results show that OPUS-Mut outperforms other methods measured by all residues, or by the interfacial

Gang Xu is a researcher at Multiscale Research Institute of Complex Systems, Fudan University. His research interests include bioinformatics and computational biology.

Yilin Wang is a student at Georgetown Preparatory School. His research interests include bioinformatics.

Qinghua Wang is a researcher at Center for Biomolecular Innovation, Harcam Biomedicines. Her research interests include structure biology.

Jianpeng Ma is a professor at Multiscale Research Institute of Complex Systems, Fudan University. He is also affiliated with Zhangjiang Fudan International Innovation Center and Shanghai AI Laboratory Shanghai. His research interests include structure biology and computational biology.

Received: May 15, 2022. **Revised:** July 17, 2022. **Accepted:** July 20, 2022

© The Author(s) 2022. Published by Oxford University Press. All rights reserved. For Permissions, please email: journals.permissions@oup.com

residues. To evaluate the performance of OPUS-Mut in scoring protein–protein docking poses, we create a protein–protein docking pose dataset Oligomer-Dock (75) using the top 10 predictions from ZDOCK 3.0.2 [27]. The results show that our scoring function OPUS-Mut (S_{all}) correctly identifies the native pose as the top-1 in 45 out of 75 targets, and ranks native pose among top-3 poses in 67 out of 75 targets. This indicates the effectiveness of using the overall side-chain packing favorableness in accordance with the local packing environment to evaluate different docking poses. In addition, we verify the performance of OPUS-Mut in studying protein mutation on an oligomeric target, SARS-CoV-2 NSP7–NSP8 complex. The results suggest that the usage of OPUS-Mut in studying protein mutation may be generalized to oligomeric complexes.

Methods

Datasets

Three oligomer datasets are collected in this study: CASP14 (11) contains 11 oligomers downloaded from the CASP14 website (https://predictioncenter.org/download_area/CASP14/targets), CAMEO-Homo (65) and CAMEO-Hetero (21) contain 65 homo-oligomers and 21 hetero-oligomers, labeled by the CAMEO website [28] released between November 2021 and February 2022, respectively. Note the oligomers with over 3000 residues in length have been excluded from the datasets because of the limitation of Graphics Processing Unit (GPU) memory. The experimental resolutions of targets in the test sets are <3.2 Å except one in CAMEO-Homo (65) [7E1B (4.6 Å)] and one in CAMEO-Hetero (21) [7B26 (3.4 Å)]. In summary, there are 63 252 residues and 18 383 interfacial residues (exclude Ala and Gly). For further evaluation, another oligomer dataset (CAMEO93o) is also included, which contains 93 oligomer targets (64 468 residues and 16 591 interfacial residues [exclude Ala and Gly]) that released between April 2022 and July 2022 from the CAMEO website.

A protein–protein docking pose dataset Oligomer-Dock (75) is created in this study. Among all 97 oligomers from three oligomer datasets, we exclude the oligomers with > 4 peptide chains, and retain 75 oligomers. For each oligomer, we use the top 10 poses generated by ZDOCK 3.0.2 [27] as its decoys. In the calculation of ZDOCK 3.0.2, for each oligomer, the last peptide chain in the Protein Data Bank (PDB) file is defined as ‘ligand’, the remaining peptide chains are defined as ‘receptor’.

OPUS-Mut

OPUS-Mut is a backbone-dependent side-chain modeling method that was released by us recently [17]. It is mainly based on OPUS-Rota4 [6], but with some improvements. The method was shown to outperform some other methods, measured by all residues or by core residues only, on the targets with single peptide chain. In our previous study [17], we use OPUS-Mut to study protein

mutation. Briefly speaking, as shown in lower green panel in Figure 1, by comparing the differences between its predicted unmutated (wild-type) side chains and its predicted mutated side chains, we can infer the extent of structural perturbation and the affected residues from those side chains significantly shifted upon the mutation. Also, from the extent of side-chain structural perturbation, we can infer the minimally disturbing mutation, from which we may construct a protein with relatively low sequence homology but with similar structure with respect to the wild type. From the affected residues, we may also use them to infer the possible functional changes if the functions are related to certain residues.

To predict the four dihedral angles of each residue, OPUS-Mut contains eight regression nodes. For each dihedral angle χ , it delivers two predictions for $\sin(\chi)$ and $\cos(\chi)$, respectively. Meanwhile, besides outputting the predicted side chain conformation, OPUS-Mut also outputs the predicted Root Mean Square Deviation (pRMSD) for its side-chain prediction (upper green panel in Figure 1). To this end, a classification node is used to learn the RMSD between the predicted side chain and its native counterpart for each residue. The pRMSD ranges from 0 to 1, and is segmented into 20 bins. The Mean Squared Error loss is used for training eight regression nodes, and the cross-entropy loss is used for training the classification node. In addition, OPUS-Mut adopts a 3DCNN module [7] to capture the local environment for each residue, therefore it can respond to the change of local environment with high sensitivity. More details of the framework of OPUS-Mut can be found in Supplementary Figure S1.

For the residue with lower pRMSD value, OPUS-Mut predicts its side chain with a higher confidence in accordance with its local environment. In this study, we use the summation of pRMSD as an indicator to gauge the overall side-chain packing favorableness in a protein structure i.e. likeliness of its local packing environment to the native packing environment. In studying docking pose, we name the summation of pRMSD over all residues as S_{all} , the summation over interfacial residues as $S_{interface}$ and the summation over other residues as S_{other} .

In our previous study, for the targets with single peptide chain, we have demonstrated that OPUS-Mut outperforms some other backbone-dependent side-chain modeling methods, measured by all residues or by core residues only. In this study, we evaluate the performance of OPUS-Mut and some other backbone-dependent side-chain modeling methods on oligomeric targets. For comparison, we also use OPUS-Mut to model each peptide chain separately i.e. to model the conformation of side chains without considering the effects of other peptide chains. We name this single-chain approach as OPUS-Mut-s.

Data availability

The code and pre-trained models of OPUS-Mut and the four datasets used in this paper can be found at

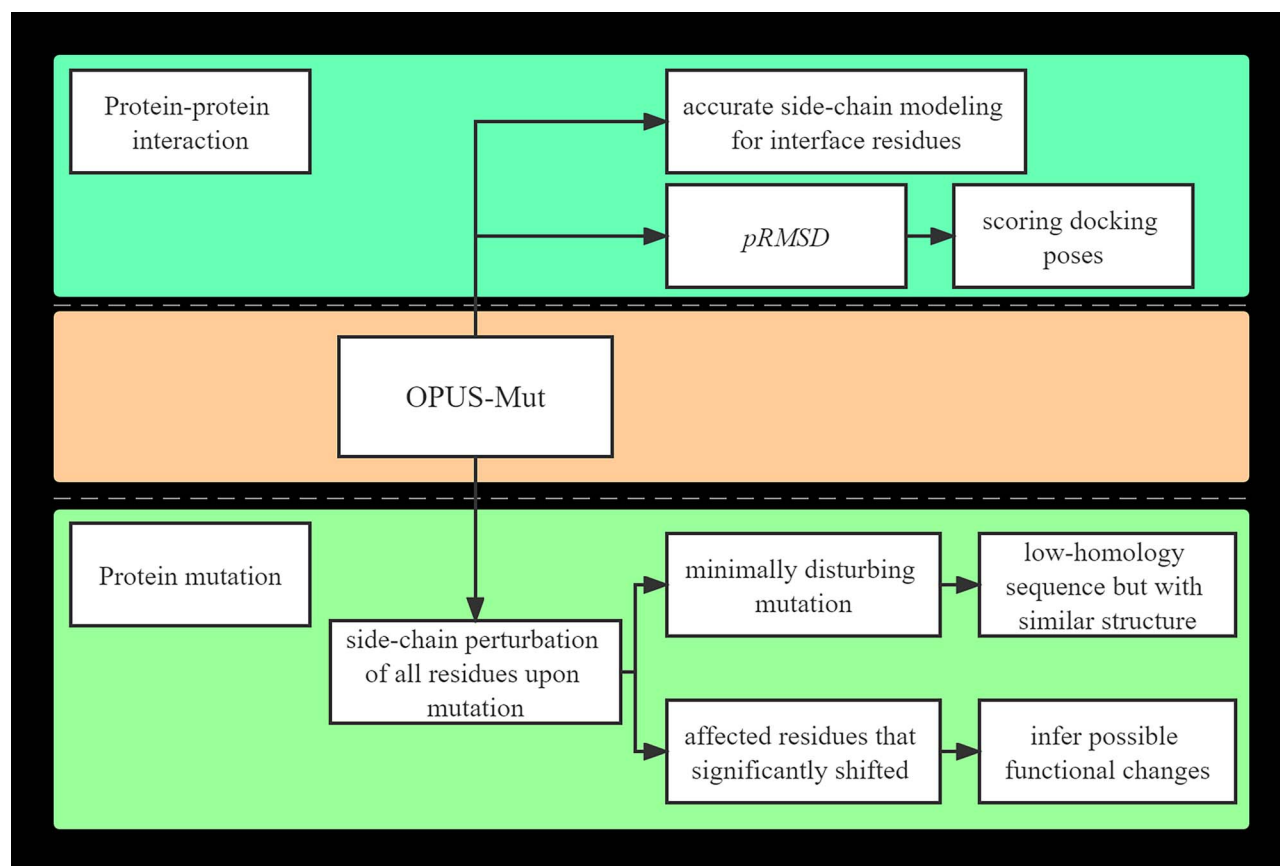


Figure 1. Two applications of backbone-dependent side-chain modeling method OPUS-Mut. The applications of OPUS-Mut in studying protein mutation on the target with single peptide chain (lower green panel) have been evaluated in our previous work. In this paper, we focus on its application in studying protein-protein interaction (upper green panel), and its application in studying protein mutation on oligomeric complexes.

http://github.com/OPUS-MaLab/opus_mut. They are freely available for academic usage only.

Results

Performance on side-chain modeling on oligomeric targets

We compare the side-chain modeling performance of OPUS-Mut with that of SCWRL4 [14], OSCAR-star [15] and DLPacker [7] on three oligomer datasets CASP14 (11), CAMEO-Homo (65) and CAMEO-Hetero (21). In terms of residue-wise percentage of correct prediction with a tolerance criterion 20° for all side-chain dihedral angles (from χ_1 to χ_4), OPUS-Mut outperforms other methods measured by all residues (Figure 2A), or by the residues located at the interfaces between different peptide chains (Figure 2B). In addition, MAE (χ_1), MAE (χ_2), MAE (χ_3) and MAE (χ_4) are used to measure the mean absolute error (MAE) of χ_1 , χ_2 , χ_3 and χ_4 between the native value and the predicted one, respectively. In terms of MAE (χ_1), MAE (χ_2), MAE (χ_3) and MAE (χ_4), OPUS-Mut also achieves the best results (Supplementary Table S1). On additional oligomer dataset CAMEO93o, OPUS-Mut also consistently outperforms other methods (Supplementary Figure S2). Meanwhile, we list the results of the percentage of correct prediction with a tolerance criterion from 10° to 40° for all side-chain dihedral angles

(from χ_1 to χ_4) of different methods measured by all residues on CAMEO93o in Supplementary Table S2. In this study, the residues with at least one nearby residue ($C_\alpha-C_\alpha$ distance $<10 \text{ \AA}$) located at other peptide chain(s) are defined as interfacial residues, and the rest residues are defined as other residues.

For example, we show two cases of OPUS-Mut side-chain modeling results on interfacial residues and their corresponding experimentally determined crystal structures in Figure 3.

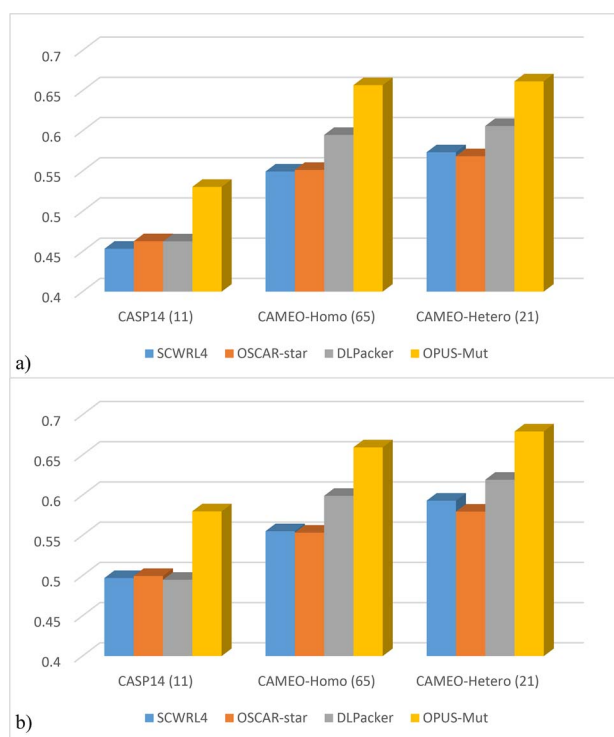
For a particular peptide chain, to evaluate the influence of other peptide chains on it, we use OPUS-Mut-s, which does not take the effect of other peptide chains into consideration, and models each peptide chain separately. As shown in Table 1, OPUS-Mut outperforms OPUS-Mut-s measured by all residues. Although the performance on other residues is almost the same, the differences are mainly seen in the interfacial residues, for which the performance of OPUS-Mut is significantly better than that of OPUS-Mut-s.

Performance on scoring protein-protein docking poses

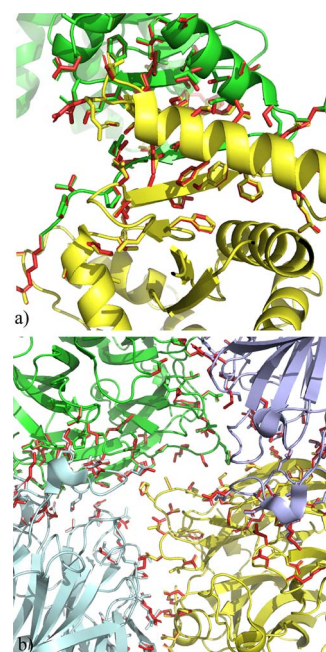
For studying protein-protein docking poses, we first examine the effect of the partner peptide chain(s) in oligomers. We compare the summation of pRMSD

Table 1. The residue-wise percentage of correct prediction with a tolerance criterion 20° for all side-chain dihedral angles (from χ_1 to χ_4) of OPUS-Mut and OPUS-Mut-s on three oligomer datasets

	All residues	Interfacial residues	Other residues
OPUS-Mut	53.02%	CASP14 (11)	49.79%
OPUS-Mut-s	49.36%	58.00%	49.48%
		49.18%	
OPUS-Mut	65.67%	CAMEO-Homo (65)	65.57%
OPUS-Mut-s	64.17%	65.95%	65.60%
		60.17%	
OPUS-Mut	66.14%	CAMEO-Hetero (21)	65.26%
OPUS-Mut-s	64.12%	67.93%	65.19%
		61.96%	

**Figure 2.** The residue-wise percentage of correct prediction with a tolerance criterion 20° for all side-chain dihedral angles (from χ_1 to χ_4) of different methods on three oligomer datasets. (A) The results measured by all residues. (B) The results measured by interfacial residues.

obtained by OPUS-Mut with that obtained by OPUS-Mut-s on three oligomer datasets, the latter does not take the effects of other peptide chains into consideration. As shown in Table 2, the average values of S_{all} of the targets in each oligomer dataset are lower than that of OPUS-Mut-s, which means the local packing environment used for side-chain prediction in OPUS-Mut is closer to native than that in OPUS-Mut-s. The average values of S_{other} between OPUS-Mut and OPUS-Mut-s are almost the same, whereas the average values of $S_{interface}$ show significant differences, which indicate that protein-protein interaction may bring a more favorable local packing environment to interfacial residues. In addition, among all 97 oligomers in three datasets, OPUS-Mut is lower than OPUS-Mut-s on 88 out of 97 targets in

**Figure 3.** Side-chain modeling results of OPUS-Mut on interfacial residues. The experimentally determined crystal structures are marked in various colors for each peptide chain. The side chains predicted by OPUS-Mut are marked in red. (A and B) The results of homo-oligomer 7DK9 and 7FIP, respectively.

terms of S_{all} , and 94 out of 97 targets in terms of $S_{interface}$, respectively.

For further investigation, we examine the performance of OPUS-Mut on distinguishing the native docking pose from 10 predicted docking pose decoys for the targets in Oligomer-Dock (75). The results of ZRANK [20] and GNN-DOVE [25] are also listed for comparison. Before the calculation of ZRANK, we use *addh* in Chimera 1.14 [29] to add the hydrogens for each PDB file, then the 'TER' line is added between ligand and receptor atom coordinates. Before the calculation of GNN-DOVE, for each PDB file, we rename the chain(s) in receptor as 'A', and the chain in ligand as 'B'. As shown in Table 3, using the summation of pRMSD over all residues [OPUS-Mut (S_{all})] as a scoring function, our method correctly identifies the native pose as the top-1 in 45 out of 75 targets, and ranks native pose among top-3 poses in 67 out of 75 targets. The

Table 2. The average values for the summation of pRMSD on three oligomer datasets

	S_{all}	$S_{interface}$	S_{other}
		CASP14 (11)	
OPUS-Mut	44.02	15.59	28.43
OPUS-Mut-s	48.49	21.16	27.33
		CAMEO-Homo (65)	
OPUS-Mut	46.05	11.90	34.15
OPUS-Mut-s	51.00	16.71	34.29
		CAMEO-Hetero (21)	
OPUS-Mut	46.59	14.12	32.47
OPUS-Mut-s	53.93	20.56	33.38

Table 3. Number of targets whose native docking poses can be successfully distinguished from their decoys in Oligomer-Dock (75) by different methods

	OPUS-Mut (S_{all})	OPUS-Mut ($M_{interface}$)	ZRANK	GNN-DOVE
TOP1	45	47	16	17
TOP3	67	61	56	29

corresponding results from ZRANK are 16 and 56, respectively. And the corresponding results from GNN-DOVE are 17 and 29, respectively. These results indicate that our scoring function, which is based on the overall side-chain packing favorableness in accordance with the local packing environment, is an effective term for scoring protein–protein docking poses.

Since the interfacial residues vary in different docking poses, we therefore use $\frac{1}{N} \sum_{n=1}^N (\text{pRMSD}_{n1} - \text{pRMSD}_{n2})$, as a scoring function [OPUS-Mut ($M_{interface}$)], to measure the extent of the improvement of the interfacial side-chain packing favorableness upon docking. For each pose, N is the number of interfacial residues, pRMSD_{n1} denotes the pRMSD of the residue n predicted by OPUS-Mut-s, pRMSD_{n2} denotes the pRMSD of the residue n predicted by OPUS-Mut. We assume that a larger $M_{interface}$ refers to a better docking pose. By using OPUS-Mut ($M_{interface}$) as a scoring function, as shown in Table 3, our method correctly identifies the native pose as the top-1 in 47 out of 75 targets and ranks native pose among top-3 poses in 61 out of 75 targets.

As examples, we show docking pose evaluation results on target T1080o in Figure 4. The score of OPUS-Mut (S_{all}) for native pose (Figure 4A) is 7.78, which is the top-1 (lowest) ranking. The scores for other decoy poses are higher e.g. 8.82 for the pose in Figure 4B, 14.54 for the pose in Figure 4C and 18.04 for the pose in Figure 4D. Moreover, in Figure 4B, the docking pose is close to the native state (DockQ [30] score 0.948), the results show that the score of ZRANK for this pose is -841.8 , lower than the native state score of -793.2 , indicating that ZRANK does not identify the correct native pose in this case, whereas ‘Ours’ does.

We also show a failed case (7LJH) in Supplementary Figure S3. The native pose of 7LJH (Supplementary Figure S3) is the fourth ranking based on the scores of OPUS-Mut (S_{all}) and is the ninth ranking based on the scores of

ZRANK. Supplementary Figure S3B–D shows three decoy poses with lower score of OPUS-Mut (S_{all}) comparing to that of the native pose. It should be noted that OPUS-Mut (S_{all}) is a scoring term that is mainly based on the local environment of side chains. Although it is effective in most cases, it has shortcomings in evaluating the docking poses from global structural point of view. Incorporating our term with other complementary terms especially those measured from global structural point of view in the future may further improve the accuracy of docking pose estimation.

Performance on studying protein mutation on oligomeric targets

Two conserved oligomer interfaces of NSP7 and NSP8 have been studied by Biswal *et al.* [31]. NSP7 and NSP8 belong to a complex of non-structural proteins (NSPs) that regulates the SARS-CoV-2 RNA-dependent RNA polymerase activity of NSP12. According to Biswal *et al.*, NSP7-NSP8 complex is mediated by two distinct oligomer interfaces: interface I responsible for hetero-dimeric NSP7-NSP8 assembly, and interface II mediating hetero-tetrameric interaction between the two NSP7-NSP8 dimers [31]. The interface I contains the following residues: K2, D5, V6, T9, L13, S15, V16, Q19, V66, I68, L71, E74, M75, Q31, F49, K51, V53, S57, L60 and S61 in NSP7, and R80, T84, M87, Q88, T89, L91, F92, R96, L98, N100, L103, I106, P116, I119, I120 and L122 in NSP 8. The interface II contains the following residues: S4, K7, C8, V11, V12, H36, N37 and L40 in NSP7, and V83, M87, M90, T93, and M94 in NSP8. In addition, some residues in interface II of the NSP7–NSP8 tetrameric complex (i.e. S4, C8, V11, V12, N37 and L40 in NSP7, and T84, M87, M90, and M94 in NSP8) are also involved in contacts with NSP12.

According to Biswal *et al.* [31], the interface I mutations NSP7^{F49A}, NSP7^{M52A}, NSP7^{L56A} and NSP8^{F92A} impair

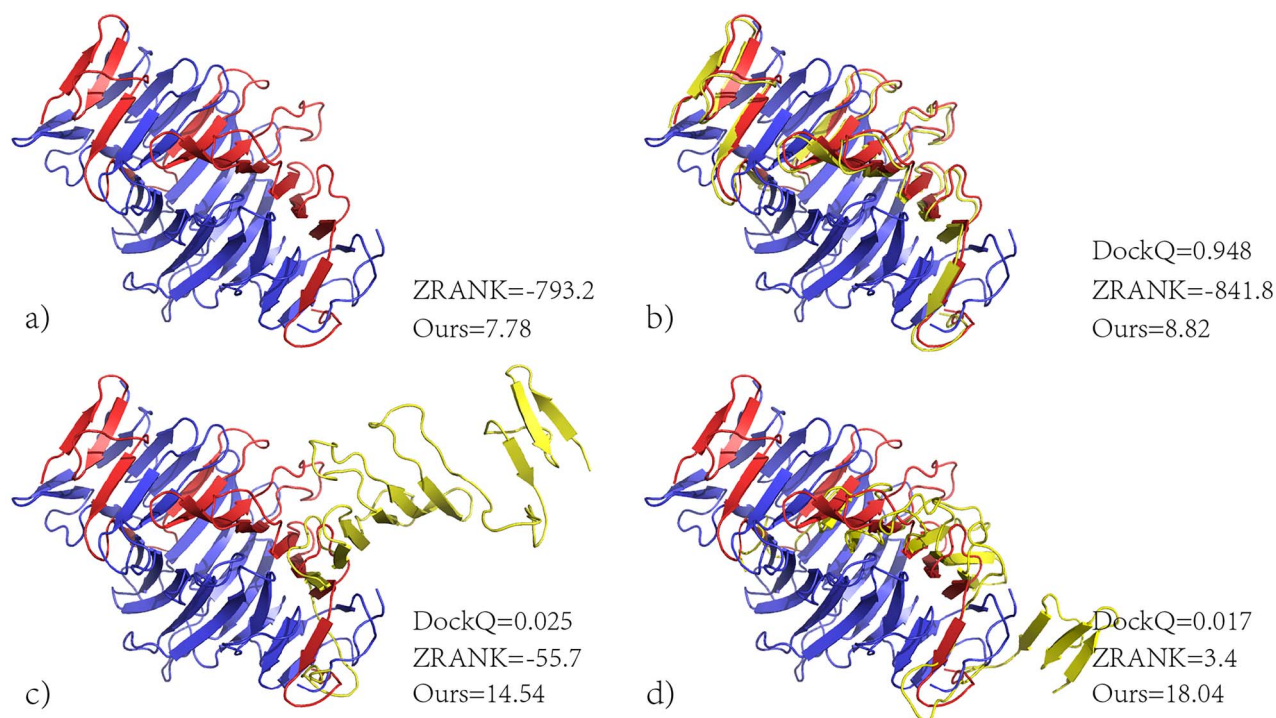


Figure 4. Docking poses evaluation results on T1080o. The structures of native receptor are marked in blue, and the structures of native ligand are marked in red. The structures of ligand predicted by ZDOCK 3.0.2 are marked in yellow. We use 'Ours' to denote the score from OPUS-Mut (S_{all}). The pose with lower score is closer to the native pose.

the NSP7–NSP8 association. The interface II mutations NSP7^{C8G}, NSP7^{V11A}, NSP8^{M90A} and NSP8^{M94A} impair the NSP7–NSP8 hetero-tetramer formation. Their results also showed that the interface II mutations lead to an even more pronounced increase of NSP8 homodimer at the expense of NSP7–NSP8 hetero-tetramer. This change is comparable or even more severe than that caused by the interface I mutations. Therefore, they concluded that interface II can not only maintain the hetero-tetrameric assembly of NSP7–NSP8, but also helps to stabilize the hetero-dimeric assembly of NSP7–NSP8 [31]. Meanwhile, the mutation NSP7^{N37V} does not affect the stability of the NSP7–NSP8 hetero-tetramer appreciably, but it leads to a modest disruption of the NSP7–NSP8–NSP12 complex [31]. According to Subissi *et al.* [32], the mutations NSP8^{K82A} and NSP8^{S85A} do not affect the NSP8–NSP12 interaction, but lead to activity loss.

In this study, we download the SARS-CoV-2 NSP7–NSP8 complex (PDB: 7JLT) [31]. Then, we substitute the residues according to the corresponding mutations mentioned above and reconstruct their side chains with OPUS-Mut. Similar to our previous study, we define the affected residue as ones whose MAE of all predicted side-chain dihedral angles (from χ_1 to χ_4) between the wild-type and mutation is greater than 5° . The rest of the side chains of other residues are deemed relatively unshifted. All of the affected residues are listed in Table 4 for each mutation, and the detailed MAE of each affected residue is listed in Supplementary Table S3.

As shown in Table 4, according to the results from OPUS-Mut, the mutation NSP7^{F49A}, NSP7^{M52A}, NSP7^{L56A}

and NSP8^{F92A} may cause significant side-chain shift of several residues involved in interface I. Mutations NSP7^{C8G}, NSP7^{V11A}, NSP8^{M90A} and NSP8^{M94A} may cause significant shift of several residues involved in both interface I and interface II, therefore may influence the function of both interface I (responsible for hetero-dimeric assembly) and interface II (mediating hetero-tetrameric interaction). Mutations NSP8^{K82A} and NSP8^{S85A} may not affect the NSP8–NSP12 interaction although both mutations are close to the residues involved in NSP8–NSP12 interaction (T84, M87, M90 and M94). The predicted results of NSP7^{N37V} are somewhat inconclusive, and the experimental results show that NSP7^{N37V} does not affect the stability of the NSP7–NSP8 hetero-tetramer appreciably although it causes a modest disruption of the NSP7–NSP8–NSP12 complex. Our predictions show NSP7^{N37V} may cause significantly shift of several residues involved in interface I, interface II and NSP8–NSP12 interface, which implies that it could affect the stability of the NSP7–NSP8 hetero-tetramer and the formation NSP7–NSP8–NSP12 complex.

Concluding discussion

Protein side chains, especially those located at the interfaces, are crucial for protein–protein interaction. In this study, we study protein–protein interaction through side-chain modeling. We evaluate the performance of several backbone-dependent side-chain modeling methods on three oligomer datasets. The results show that our previous released method OPUS-Mut [17] outperforms other

Table 4. Affected residues of different mutations predicted by OPUS-Mut and catalogized by their locations.

	Interface I	Interface II	NSP8-NSP12	Others
NSP7 ^{F49A}	K2, V6, V66, M75			M3, T45, M52, S25
NSP7 ^{M52A}	V66, K51			
NSP7 ^{L56A}	T9, V66			M52
NSP8 ^{F92A}	L71, V66, Q88			
NSP7 ^{C8G}	V66	M90, T93, M94	M90, M94	S25, R79, T81
NSP7 ^{V11A}	T9, S15, Q19, R80, M87, M75	H36, M87	M87	R21, E23, M52, D78, S25, Q34
NSP8 ^{M90A}	V66, M75	T93		S85, T81
NSP8 ^{M94A}	T9, L71	T93		M52, S85
NSP7 ^{N37V}	T9, Q19, R80, M75, M87	H36, L40, M87	L40, M87	R21, E23, Q34, S25
NSP8 ^{K82A}				E77
NSP8 ^{S85A}	V66, M75			

Experimentally, on the interface I, mutations NSP7^{F49A}, NSP7^{M52A}, NSP7^{L56A} and NSP8^{F92A} impair the NSP7–NSP8 association; on the interface II, mutations NSP7^{C8G}, NSP7^{V11A}, NSP8^{M90A} and NSP8^{M94A} impair the NSP7–NSP8 hetero-tetramer formation. The interface II maintains the hetero-tetrameric assembly of NSP7–NSP8, and also stabilizes the hetero-dimeric assembly of NSP7–NSP8. The mutation NSP7^{N37V} does not destabilize the stability of the NSP7–NSP8 hetero-tetramer significantly, but causes a modest disruption of the NSP7–NSP8–NSP12 complex. The mutations NSP8^{K82A} and NSP8^{S85A} do not affect the NSP8–NSP12 interaction, but result in activity loss.

methods measured by all residues or by the interfacial residues (Figure 2), and its side-chain modeling results for the residues located between different peptide chains are very close to their experimentally determined crystal structures (Figure 3).

When omitting the influence of partner peptide chain(s) in an oligomer and modeling the side chains of each peptide chain separately, the modeling accuracy on oligomer will decrease, especially for that on interfacial residues (OPUS-Mut-s, Table 1). This result indicates that the side chains of interfacial residues may experience conformational changes upon protein–protein association, and it also demonstrates the sensitivity of OPUS-Mut towards local environmental changes.

OPUS-Mut can output the pRMSD for its predicted side chains on each residue. For a particular residue, lower pRMSD value indicates that OPUS-Mut predicts its side chain with a higher confidence in accordance with its local environment. In this study, we use the summation of pRMSD as an indicator to gauge the overall packing favorableness of side-chain in a protein structure i.e. likeliness of its local packing environment to the native packing state.

As shown in Table 2, the average values of the summation of pRMSD over all residues (S_{all}) obtained by OPUS-Mut are lower than that obtained by OPUS-Mut-s. The average values of S_{other} between OPUS-Mut and OPUS-Mut-s are almost the same, whereas the average values of $S_{interface}$ show significant differences. Among all 97 oligomers in three datasets, OPUS-Mut is lower than OPUS-Mut-s on 88 out of 97 targets in terms of S_{all} , and 94 out of 97 targets in terms of $S_{interface}$, respectively. The results indicate that protein–protein interaction may bring a more favorable local packing environment to the interfacial residues.

We compare the performance of identifying native docking pose based on pRMSD from OPUS-Mut with that of ZRANK and GNN-DOVE on Oligomer-Dock (75). Using the summation of pRMSD over all residues [OPUS-Mut (S_{all})] as a scoring function achieves better results than

that using the result from ZRANK and GNN-DOVE, either on correctly identifying native pose, or on ranking native pose in the top three poses (Table 3). The deep learning-based binary classification model (0 for incorrect pose, and 1 for near-native pose) such as GNN-DOVE is capable of distinguishing the near-native poses from the incorrect poses; however, they cannot effectively distinguish the native pose from the near-native decoys. In contrast, as shown in Figure 4, our scoring function OPUS-Mut (S_{all}), which is based on the confidence of local side-chain packing environment, can correctly identify the native pose (Figure 4A) from the near-native pose (Figure 4B, DockQ=0.948). Thus, it may be an effective and complementary scoring term for studying protein–protein interaction, especially for identifying the native pose from its decoys, including those near-native decoys.

Note that, using the summation of pRMSD on interfacial residues as a scoring function [OPUS-Mut ($M_{interface}$)] may have a bias since the interfacial residues vary in different docking poses. Therefore, we recommend using OPUS-Mut (S_{all}) as a scoring function for scoring different poses.

We also verify the performance of OPUS-Mut in studying protein mutation on oligomeric target, SARS-CoV-2 NSP7–NSP8 complex. As shown in Table 4, most of our results are consistent with the experimental results, which indicate that the usage of OPUS-Mut in studying protein mutation may be generalized to oligomeric target. Therefore, based on the predicted side-chain structural perturbation upon mutation, our methods may be helpful to infer the possible functional changes of the mutation on the interface between two proteins, which is beneficial to protein engineering.

For side-chain modeling, OPUS-Mut, as well as other backbone dependent side-chain modeling methods, requires backbone as its input, whereas AlphaFold2 only requires the sequence as its input. As shown in Supplementary Table S4, when using the native backbone as its input, OPUS-Mut significantly outperforms AlphaFold2 on both monomer targets and oligomer targets measured

by side-chain modeling accuracy. In addition, OPUS-Mut is more helpful if one wishes to construct the side chains on a given backbone.

For modeling oligomer target, AlphaFold2 can predict the structure using the sequence information only. There is, however, still a gap between the prediction of AlphaFold2 and the native structure (e.g. TM-score = 0.66 for CASP14 (11) in [Supplementary Table S4](#)), whereas the docking method, such as ZDOCK, which uses the structures of receptor and ligand as its inputs, achieves better results [the best TM-score of the top-10 ZDOCK predictions for CASP14 (11) is 0.92]. In this case, our scoring function OPUS-Mut (S_{all}) correctly identifies the native pose as the top-1 or top-3 which is better than those from ZRANK and GNN-DOVE, and therefore OPUS-Mut (S_{all}) may be a useful term in helping the docking method for the estimation of docking pose due to its effectiveness of identifying the native pose from its decoys, including those near-native decoys.

Key Points

- We evaluate the performance of several backbone-dependent side-chain modeling methods on three oligomer datasets. The results show that our previous released method OPUS-Mut outperforms other methods measured by all residues or by the interfacial residues. The results also demonstrate the sensitivity of OPUS-Mut towards local side-chain packing environment.
- We propose a scoring function for protein-protein docking pose assessment, OPUS-Mut (S_{all}), which is based on the overall side-chain packing favorableness in accordance with the local packing environment. The results show that it correctly identifies the native pose as the top-1 in 45 out of 75 targets and ranks native pose among top-3 poses in 67 out of 75 targets. This indicates its possibility to be a new and effective scoring term for studying protein-protein interaction.
- We verify the performance of OPUS-Mut in studying protein mutation on oligomeric target, SARS-CoV-2 NSP7-NSP8 complex. The results suggest that the usage of OPUS-Mut in studying protein mutation may be generalized to oligomeric complexes.
- To facilitate the research in the field, the code of OPUS-Mut and the datasets collected in this paper can be downloaded at http://github.com/OPUS-MaLab/opus_mut.

Supplementary data

Supplementary data are available online at <https://academic.oup.com/bib>.

Funding

Shanghai Municipal Science and Technology Major Project (No. 2018SHZDZX01), and ZJLab. The work was also supported by National Key Research and Development Program of China (No. 2021YFF1200400).

References

1. Wang B, Mei C, Wang Y, et al. Imbalance data processing strategy for protein interaction sites prediction. *IEEE/ACM Trans Comput Biol Bioinform* 2021;**18**:985–94.
2. Esmailbeiki R, Krawczyk K, Knapp B, et al. Progress and challenges in predicting protein interfaces. *Brief Bioinform* 2016;**17**:117–31.
3. Wang C, Schueler-Furman O, Baker D. Improved side-chain modeling for protein-protein docking. *Protein Sci* 2005;**14**:1328–39.
4. Zhao Y, Sanner MF. Protein-ligand docking with multiple flexible side chains. *J Comput Aided Mol Des* 2008;**22**:673–9.
5. Xu G, Wang Q, Ma J. OPUS-Rota3: improving protein side-chain modeling by deep neural networks and ensemble methods. *J Chem Inf Model* 2020;**60**:6691–7.
6. Xu G, Wang Q, Ma J. OPUS-Rota4: a gradient-based protein side-chain modeling framework assisted by deep learning-based predictors. *Brief Bioinform* 2022;**23**(3):bbac130.
7. Misiura M, Shroff R, Thyer R, et al. DLPacker: deep learning for prediction of amino acid side chain conformations in proteins. *Proteins* 2022;**90**:1278–90.
8. Cao Y, Song L, Miao Z, et al. Improved side-chain modeling by coupling clash-detection guided iterative search with rotamer relaxation. *Bioinformatics* 2011;**27**:785–90.
9. Huang X, Pearce R, Zhang Y. FASPR: an open-source tool for fast and accurate protein side-chain packing. *Bioinformatics* 2020;**36**:3758–65.
10. Liang S, Zhou Y, Grishin N, et al. Protein side chain modeling with orientation-dependent atomic force fields derived by series expansions. *J Comput Chem* 2011;**32**:1680–6.
11. Lu M, Dousis AD, Ma J. OPUS-Rota: a fast and accurate method for side-chain modeling. *Protein Sci* 2008;**17**:1576–85.
12. Miao Z, Cao Y, Jiang T. RASP: rapid modeling of protein side chain conformations. *Bioinformatics* 2011;**27**:3117–22.
13. Nagata K, Randall A, Baldi P. SIDEpro: a novel machine learning approach for the fast and accurate prediction of side-chain conformations. *Proteins* 2012;**80**:142–53.
14. Krivov GG, Shapovalov MV, Dunbrack RL, Jr. Improved prediction of protein side-chain conformations with SCWRL4. *Proteins* 2009;**77**:778–95.
15. Liang S, Zheng D, Zhang C, et al. Fast and accurate prediction of protein side-chain conformations. *Bioinformatics* 2011;**27**:2913–4.
16. Xu G, Ma T, Du J, et al. OPUS-Rota2: an improved fast and accurate side-chain modeling method. *J Chem Theor Comput* 2019;**15**:5154–60.
17. Xu G, Wang Q, Ma J. OPUS-Mut: studying the effect of protein mutation through side-chain modeling. *bioRxiv*. 2022; 2022.2005.2010.491420.
18. Sunny S, Jayaraj PB. Protein-protein docking: past, present, and future. *Protein J* 2022;**41**:1–26.
19. Feng T, Chen F, Kang Y, et al. HawkRank: a new scoring function for protein-protein docking based on weighted energy terms. *J Chem* 2017;**9**:66.
20. Pierce B, Weng Z. ZRANK: reranking protein docking predictions with an optimized energy function. *Proteins* 2007;**67**:1078–86.
21. Roy AA, Dhawanjewar AS, Sharma P, et al. Protein Interaction Z Score Assessment (PIZSA): an empirical scoring scheme for evaluation of protein-protein interactions. *Nucleic Acids Res* 2019;**47**:W331–7.
22. Huang SY, Zou X. An iterative knowledge-based scoring function for protein-protein recognition. *Proteins* 2008;**72**:557–79.
23. Moal IH, Barradas-Bautista D, Jimenez-Garcia B, et al. IRAPPA: information retrieval based integration of biophysical

- models for protein assembly selection. *Bioinformatics* 2017;**33**:1806–13.
24. Wang X, Terashi G, Christoffer CW, et al. Protein docking model evaluation by 3D deep convolutional neural networks. *Bioinformatics* 2020;**36**:2113–8.
 25. Wang X, Flannery ST, Kihara D. Protein docking model evaluation by graph neural networks. *Front Mol Biosci* 2021;**8**:647915.
 26. Geng CL, Jung Y, Renaud N, et al. iScore: a novel graph kernel-based function for scoring protein-protein docking models. *Bioinformatics* 2020;**36**:112–21.
 27. Pierce BG, Hourai Y, Weng Z. Accelerating protein docking in ZDOCK using an advanced 3D convolution library. *PLoS One* 2011;**6**:e24657.
 28. Haas J, Barbato A, Behringer D, et al. Continuous Automated Model EvaluatiOn (CAMEO) complementing the critical assessment of structure prediction in CASP12. *Proteins Struct Funct Bioinform* 2018;**86**:387–98.
 29. Pettersen EF, Goddard TD, Huang CC, et al. UCSF chimera – a visualization system for exploratory research and analysis. *J Comput Chem* 2004;**25**:1605–12.
 30. Basu S, Wallner B. DockQ: a quality measure for protein-protein docking models. *PLoS One* 2016;**11**:e0161879.
 31. Biswal M, Diggs S, Xu D, et al. Two conserved oligomer interfaces of NSP7 and NSP8 underpin the dynamic assembly of SARS-CoV-2 RdRP. *Nucleic Acids Res* 2021;**49**:5956–66.
 32. Subissi L, Posthuma CC, Collet A, et al. One severe acute respiratory syndrome coronavirus protein complex integrates processive RNA polymerase and exonuclease activities. *Proc Natl Acad Sci U S A* 2014;**111**:E3900–9.